Available online at www.sciencedirect.com
ScienceDirect
Journal of Power Sources 159 (2006) 1340–1345
JOURNAL OF POWER SOURCES
www.elsevier.com/locate/jpowsour

Low temperature performance of nanophase $Li_4Ti_5O_{12}$

J.L. Allen *, T.R. Jow, J. Wolfenstine

U.S. Army Research Laboratory, Adelphi, MD 20783-1197, USA

Received 2 November 2005; received in revised form 7 December 2005; accepted 8 December 2005
Available online 25 January 2006

Abstract

The low temperature electrochemical performances of 700 and 350 nm $Li_4Ti_5O_{12}$ were compared. At high rate, room temperature and at low rate and low temperature (0, −10, −20 and −30 °C), the 350 nm $Li_4Ti_5O_{12}$ showed higher capacity than the 700 nm $Li_4Ti_5O_{12}$. This difference is proposed to result from the shorter diffusion lengths and higher number of lithium insertion sites in the 350 nm $Li_4Ti_5O_{12}$ compared to the 700 nm $Li_4Ti_5O_{12}$. However, at high rate and low temperature, a transition in performance was observed, that is, the 700 nm material had higher capacity. At high rate and low temperature, it is proposed that interparticle contact resistance becomes rate limiting owing to the temperature dependence of this property and this accounts for the different behavior at low temperature and high rate.
Published by Elsevier B.V.

Keywords: $Li_4Ti_5O_{12}$; Anode; Li-ion battery; Low temperature; Nanophase

1. Introduction

$Li_4Ti_5O_{12}$ is a potential anode material for Li-ion batteries with some unique and potentially useful characteristics [1–3]. For example, it is a zero-strain lithium insertion host suggesting virtually unlimited cycle life. It features a flat, operating voltage of about 1.5 V versus lithium, above the reduction potential of common electrolyte solvents thus, it does not form a solid electrolyte interface based on solvent reduction which should be a favorable property for high rate and low temperature operation. This voltage also is sufficiently high such that the dangers of lithium plating that can occur at high rate and/or low temperature are removed. The use of nanophase $Li_4Ti_5O_{12}$ has been shown to yield improvements in rate capability [4–6]. Furthermore, the use of nanostructured electrodes has been reported to enhance low temperature performance [7–9]. Up to this time, the low temperature performance of nanophase $Li_4Ti_5O_{12}$ has not been reported. Herein, we report on the low temperature performance as a function of particle size and rate.

2. Experimental

Two $Li_4Ti_5O_{12}$ samples were compared of differing particle size: (1) Nanomyte^{TM} $Li_4Ti_5O_{12}$, obtained from NEI corporation, hereafter referred to as NEI-$Li_4Ti_5O_{12}$ [10] (2) a larger particle size $Li_4Ti_5O_{12}$ prepared at ARL using a solid-state method [11] from TiO_2 (rutile structure) and Li_2CO_3, hereafter referred to as ARL-$Li_4Ti_5O_{12}$. Three weight percent excess Li_2CO_3 was used to compensate for lithia volatilization during the high temperature heating. The starting materials were ground with an alumina mortar and pestle with enough methanol to form a slurry. The dried and mixed reactant mixture was heated at 800 °C for 12 h in air. The sample was reground, pelletized and heated for another 24 h at 800 °C in air.

The $Li_4Ti_5O_{12}$ samples were first characterized by X-ray diffraction with a Rigaku Ultima III diffractometer using Cu Kα radiation. Lattice constants were determined by obtaining diffraction data in a parallel beam diffraction geometry and fitting the data using Rietveld refinement [12] using RIQAS software (Materials Data Inc.). Crystal size was evaluated by collecting diffraction data in a Bragg–Brentano (focusing) geometry and correcting for instrumental broadening by using LaB_6 (NIST; 660A).

Surface area measurements were done by the Brunauer–Emmett–Teller (BET) [13] method using N_2 as adsorbate gas. The average particle size diameter was calculated based on this

* Corresponding author. Tel.: +1 301 394 0291; fax: +1 301 394 0273.
E-mail address: jallen@arl.army.mil (J.L. Allen).

0378-7753/$ – see front matter. Published by Elsevier B.V.
doi:10.1016/j.jpowsour.2005.12.039

surface area assuming a spherical particle [14]. Particle size and morphology were also evaluated using scanning (SEM) and transmission (TEM) electron microscopy.

For electrochemical testing, a composite electrode with a load of $2.10 \pm 0.05\ mg\ cm^{-2}$ was fabricated by a slurry coating method. Using γ-butyrolactone as solvent, a slurry of 78 wt.% $Li_4Ti_5O_{12}$, 12 wt.% polyvinylidene fluoride and 10 wt.% super-P carbon was prepared and coated onto an aluminum foil substrate. The electrode film was cut into small discs with an area of $0.97\ cm^2$ and dried at 60 °C in air before use. In a dry room (dew point < −80 °C), Li/$Li_4Ti_5O_{12}$ button cells were assembled using Celgard 3501 membrane as the separator and a 1.0 M $LiPF_6$ solution in a 1:1 (wt.%) mixture of propylene carbonate (PC) and 1,2-dimethoxyethane (DME) electrolyte. A Tenney Environmental Oven was used to provide constant temperature at 20, 0, −10, −20, and −30 °C. Cycling testing was performed using a Maccor Series 4000 tester. The cells were cycled between 3.0 and 1.0 V at C-rates from 0.1 to 5.

3. Results and discussion

Fig. 1 compares the powder X-ray diffraction patterns of the NEI-$Li_4Ti_5O_{12}$ and the ARL-$Li_4Ti_5O_{12}$ materials. Careful inspection of the patterns shows no evidence of rutile ($2\theta \approx 27°$) or anatase ($2\theta \approx 25°$) polymorphs of TiO_2, impurities commonly observed in $Li_4Ti_5O_{12}$ samples. The lattice constants as determined from Rietveld analysis of the XRD pattern are 8.35610 (±0.00004) Å and 8.35575 (±0.00005) Å for ARL-$Li_4Ti_5O_{12}$ and NEI-$Li_4Ti_5O_{12}$, respectively. These lattice constants are similar to values obtained for $Li_4Ti_5O_{12}$ obtained via high temperature syntheses: 8.369 Å [15], 8.367 Å [1], 8.365 Å [3], 8.358 Å [16] and 8.357 Å [8].

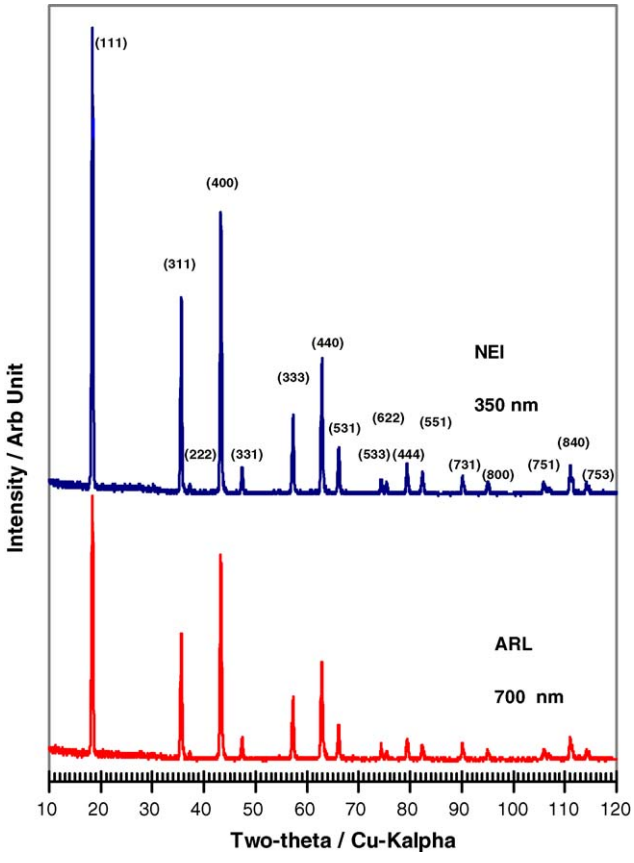

Fig. 1. X-ray diffraction patterns of NEI-$Li_4Ti_5O_{12}$ and ARL-$Li_4Ti_5O_{12}$.

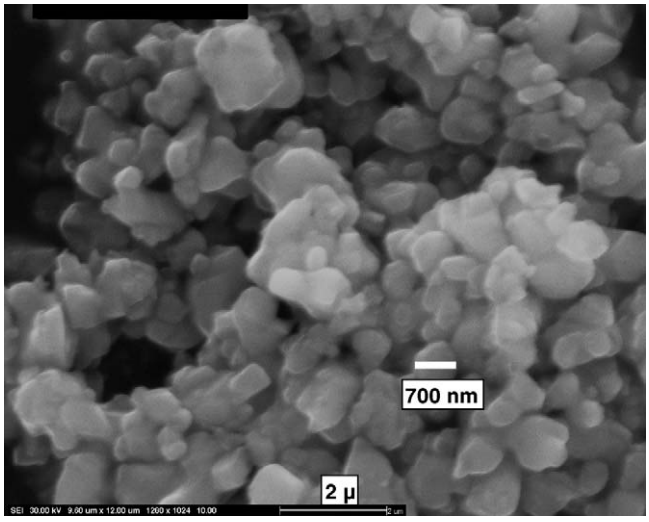

Fig. 2. Scanning electron micrograph of ARL-$Li_4Ti_5O_{12}$.

The average crystal size was estimated for NEI-$Li_4Ti_5O_{12}$ from measurement of the broadening of the X-ray reflections. Using the Scherrer formula [17]:

$$t = \frac{0.9\lambda}{B\cos\theta_B}, \quad (1)$$

where t is the thickness of the crystal in angstroms, λ the wavelength of the radiation, and B is the line broadening. B was calculated from the Warren formula [17]:

$$B^2 = B_M^2 - B_S^2 \quad (2)$$

using LaB_6 as the line broadening standard, where B_M is the sample peak full width half maximum (FWHM) and B_S the FWHM of the LaB_6 standard. From these measurements a crystal size of 230 nm was calculated. ARL-$Li_4Ti_5O_{12}$ has a crystal size too large to be measured via X-ray reflection line broadening.

Fig. 2 is an SEM image of ARL-$Li_4Ti_5O_{12}$. The SEM image shows a fairly uniform particle size of about 700 nm. The morphology can be reasonably approximated as equiaxed. Fig. 3 is a TEM image of NEI-$Li_4Ti_5O_{12}$. The TEM image of NEI-$Li_4Ti_5O_{12}$ shows equiaxed particles of about 350 nm diameter.

BET surface areas of 2.46 and $4.85\ m^2\ g^{-1}$ were measured for ARL-$Li_4Ti_5O_{12}$ and NEI-$Li_4Ti_5O_{12}$, respectively. The average particle size diameter was calculated based on this surface area assuming a spherical particle using the equation [14]:

$$d = \frac{6}{\rho S_{BET}} \quad (3)$$

where d is the particle size, ρ the density of $Li_4Ti_5O_{12}$ ($3.5\ g\ mL^{-1}$) and S_{BET} is the BET surface area [14].

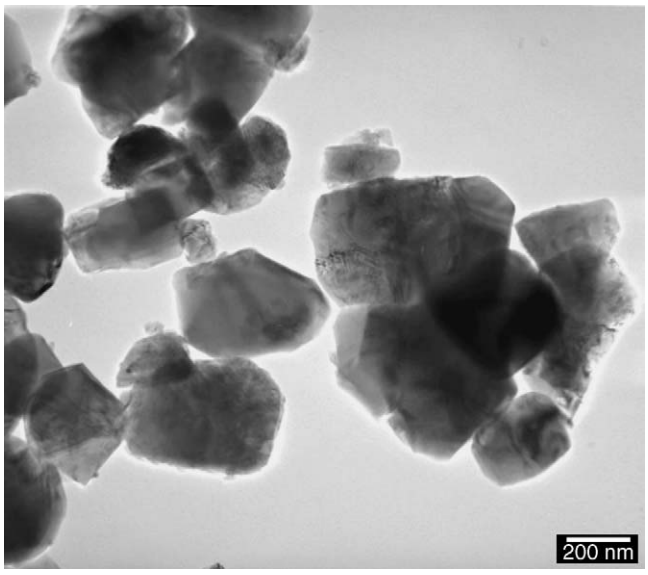

Fig. 3. Transmission electron micrograph of NEI-$Li_4Ti_5O_{12}$.

The characterization of the two samples is summarized in Table 1.

All of the characterization methods are in close agreement and thus, we assign an average particle size of ca. 700 nm for ARL-$Li_4Ti_5O_{12}$ and ca. 350 nm for NEI-$Li_4Ti_5O_{12}$.

Fig. 4 compares the capacity and voltage of ARL-$Li_4Ti_5O_{12}$ and NEI-$Li_4Ti_5O_{12}$ as a function of temperature at a low rate of 0.06 mAh cm^{-2} (C rate ≈ C/8). The temperature ranges are coded by color and symbols: red squares, black diamonds, green triangles, blue circles and purple asterisks corresponding to 20, 0, −10, −20 and −30 °C, respectively. Solid lines and symbols correspond to ARL-$Li_4Ti_5O_{12}$ and dashed lines and hollow symbols correspond to NEI-$Li_4Ti_5O_{12}$. The theoretical capacity of $Li_4Ti_5O_{12}$ is 175 mAh g^{-1} per the following lithium insertion reaction:

$$Li_4Ti_5O_{12} + 3Li^+ + 3e^- \rightarrow Li_7Ti_5O_{12} \quad (4)$$

Both samples showed near 90% of the theoretical capacity: at 20 °C, ARL-$Li_4Ti_5O_{12}$ (red dashed line, Fig. 4) had a specific capacity of 163 mAh g^{-1} and NEI-$Li_4Ti_5O_{12}$ (solid red line, Fig. 4) had a specific capacity of 152 mAh g^{-1}. The slight difference in baseline capacity may result from the fact that the electrode film processing method was developed for micrometer sized materials and may need to be adjusted to account for the use of smaller particles. The voltage of discharge for both samples is 1.5 V, indicating no difference in polarization and

Table 1
Particle size characterization

Method	ARL-$Li_4Ti_5O_{12}$	NEI-$Li_4Ti_5O_{12}$
XRD	N/A	ca. 230 nm (crystal size)
SEM	ca. 700 nm	N/A
TEM	N/A	ca. 350 nm
BET	700 nm	353 nm

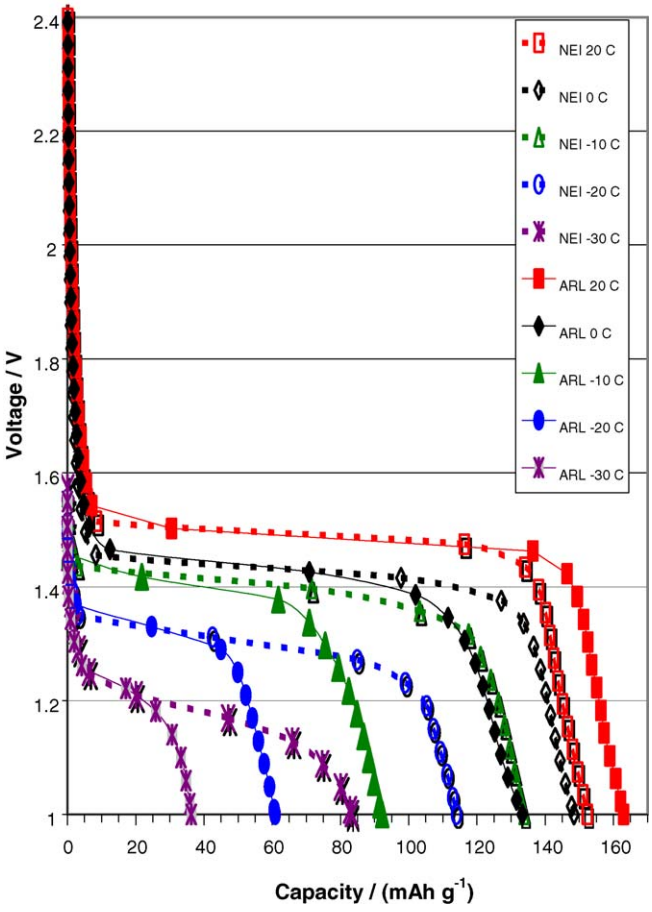

Fig. 4. Discharge curves of ARL-$Li_4Ti_5O_{12}$ (solid) and NEI-$Li_4Ti_5O_{12}$ (dashed)as a function of temperature at rate of 0.06 mAh cm^{-2} (≈C/8).

in agreement with literature values [1–3] for the insertion of lithium into $Li_4Ti_5O_{12}$. When the temperature was lowered to 0 °C, we immediately see the effect of the smaller particle size of NEI-$Li_4Ti_5O_{12}$. The specific capacity of NEI-$Li_4Ti_5O_{12}$ was 148 mAh g^{-1}, representing a 3% drop in capacity, whereas, the capacity of ARL-$Li_4Ti_5O_{12}$ dropped to 133 mAh g^{-1}, an 18% drop in capacity. This demonstrates the powerful effect of decreasing particle size upon the kinetics of lithium insertion as temperature is lowered. This is even more evident at −30 °C, the NEI-$Li_4Ti_5O_{12}$ is still delivering more than 83 mAh g^{-1}, whereas, the larger particle size ARL-$Li_4Ti_5O_{12}$ only delivers 36 mAh g^{-1}. This supports the hypothesis that scaling down the particle size can improve low rate temperature performance through shortened diffusion lengths and the larger number of lithium insertion sites that result from the increased surface area. The observation that higher $Li_4Ti_5O_{12}$ capacity is maintained with decreasing particle size, as temperature is lowered, is in agreement with results of Huang et al [7,8] on coke and Slides and Martin [9] on V_2O_5 nanorods. Both sets of authors observed that as particle size decreases, more capacity is maintained at low temperature.

What happens when the discharge rate is increased? Fig. 5 compares the normalized capacity for ARL-$Li_4Ti_5O_{12}$ and NEI-$Li_4Ti_5O_{12}$ as a function of rate (from C/8 to 5C) at various

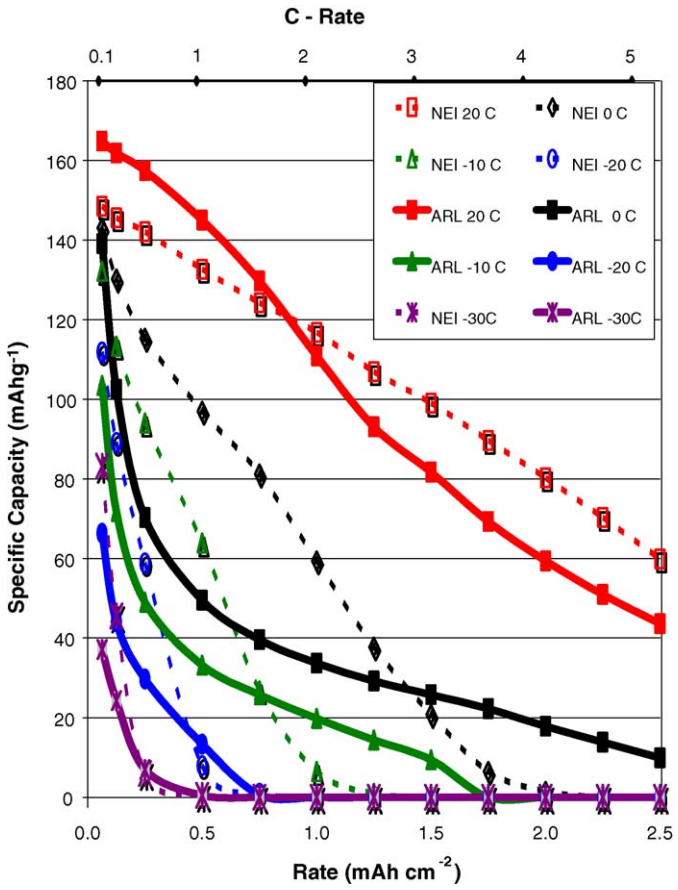

Fig. 5. Normalized capacity as a function of discharge rate for ARL-$Li_4Ti_5O_{12}$ (solid) and NEI-$Li_4Ti_5O_{12}$ (dashed).

temperatures. The capacity is normalized with respect to the room temperature capacity. This was done to make trends in the data clearer. This is justified in the fact that the room temperature capacities for the two materials (163 mAh g^{-1} versus 152 mAh g^{-1}) differ by less than 7%. In this figure, we follow the same color code and dashed/solid conventions as in Fig. 4. From Fig. 5, it can be seen that at room temperature and at low rates up to 1C, the ARL-$Li_4Ti_5O_{12}$ and NEI-$Li_4Ti_5O_{12}$, have about the same normalized capacity but as the rate increase above 1C to 5C, the smaller particle size NEI-$Li_4Ti_5O_{12}$ exhibits a significantly higher normalized capacity compared to ARL-$Li_4Ti_5O_{12}$ and this difference increases as rate increases. However, as temperature is lowered, there is a change between which of the materials has the higher capacity as the discharge rate increases. At room temperature, the NEI-$Li_4Ti_5O_{12}$ has higher capacity at all rates tested (from C/8 to 5C) but during low temperature testing ($T \leq 0\,^{\circ}C$), when rate is increased, there is a cross-over rate at which the ARL-$Li_4Ti_5O_{12}$ has the higher capacity. From Fig. 5, it is seen that as temperature decreases, this cross-over rate decreases to a lower discharge rate.

At present, reasons for this transition are uncertain. We can speculate on the reasons for the transition by (1) considering what is different between NEI-$Li_4Ti_5O_{12}$ and ARL-$Li_4Ti_5O_{12}$, (2) considering the effects of the differences and (3) determining, based on the effects, if the difference leads to a plausible explanation. The first difference we consider is surface area. The NEI-$Li_4Ti_5O_{12}$ has approximately two times the surface area of ARL-$Li_4Ti_5O_{12}$. This property will not change as temperature is lowered and, in fact, should lead to better low temperature [7,8], high rate performance for NEI-$Li_4Ti_5O_{12}$ since the number of insertion sites is directly proportional to the surface area. Therefore, this difference can be excluded as a reason for the transition. The second difference we consider is particle diameter: NEI-$Li_4Ti_5O_{12}$ has a particle diameter half that of ARL-$Li_4Ti_5O_{12}$. This difference means that the lithium ion diffusion lengths will be shorter for the NEI material and should improve low temperature-high rate performance [7–9]. Thus, we can also exclude this difference as a reason for the transition. Third, we can consider the different methods of synthesis: the NEI-$Li_4Ti_5O_{12}$ was made at a lower temperature and therefore one might speculate that there exists a greater possibility that because of the low temperature of synthesis some amorphous or other non-equilibrium phase is present [18]. The ARL-$Li_4Ti_5O_{12}$, synthesized at a higher temperature, is more likely to be fully reacted and contain only the thermodynamically most stable phase, which is presumably $Li_4Ti_5O_{12}$ [18]. This possible difference in the two samples may have some effect on the low temperature high rate performance but it is not readily apparent how this would change the low temperature-high rate performance and there is no evidence to support the presence of such a phase or amorphous component. One could also speculate that the differences in synthesis may affect the surface chemistry. But again, it is not readily apparent how this would affect the low temperature high rate performance and we have no evidence of differences in the surface chemistry. Elucidation of possible differences would require considerable experimental work beyond the scope of this paper. Thus, we will conclude that the difference in synthesis may have some effect but we will reasonably conclude that it is probably not the reason for the transition. Fourth, we consider processing of the electrode composite. The two active materials were processed in an identical fashion but it is a processing method developed for micrometer-sized particles. However, at room temperature, the NEI-$Li_4Ti_5O_{12}$ outperforms the ARL-$Li_4Ti_5O_{12}$ and non-optimal processing should affect the room temperature performance as well as the low temperature performance. Even with optimal processing, the smaller particle size material will still have more interparticle contacts. We do not want to minimize the importance of processing, because the processing of nanoparticle based electrodes needs to be optimized, but we do not see it as a probable explanation for the cross-over phenomenon. Finally, we consider the effect of $Li_4Ti_5O_{12}$ inter-particle contacts. Owing to the fact that the NEI-$Li_4Ti_5O_{12}$ is approximately half the diameter of ARL-$Li_4Ti_5O_{12}$ there will be a proportional increase in the number of inter-particle contacts for a given volume of NEI-$Li_4Ti_5O_{12}$ versus ARL-$Li_4Ti_5O_{12}$. This leads to the question of whether we should consider an interfacial phenomeon arising from the formation of a solid electrolyte interface (SEI) or do differences in performance result from interparticle resistances. The SEI is generally agreed to be a result of the reduction of elec-

trolytes on the surface of the electrode to form a passivating layer that prevents further electrolyte reduction. It generally starts forming at 0.8 V for PC based electrolytes and much lower for ether type solvents such as DME [19]. Since we cycle between 3 and 1 V, we will assume that since we are above the reduction potential of the electrolyte, there is no SEI formation. We assume then that the interparticle effects will be electronic in nature. Further experiments using electrochemical impedance spectroscopy are planned to test this assumption.

Now, we turn our focus onto the electronic resistance. During charge and discharge, electrons are transferred from particle to particle. Each transfer of electrons has a resistivity associated with this process. The effect of introducing interparticle contacts causes an increase in the overall resistance because of the increased number of interparticle contacts, each of which has its own resistance. Could this be part of the explanation for the transition? Well, resistance is a property, which varies (often exponentially [20]) as a function of temperature and if we assume that the interparticle resistance increases as temperature is lowered then one reasonable explanation for the transition is that the higher number of interparticle contacts in the NEI material compared to the ARL material leads to a higher overall resistance. This resistance is not significant at higher temperatures but this resistance becomes more important at low temperature because electronic resistance of semiconductors and insulators is significantly higher at low temperature [20]. At room temperature, another step is rate limiting. Owing to the fact that the smaller particle NEI material has better rate performance at room temperature, we suggest that the room temperature rate is limited by either intraparticle lithium ion diffusion or the number available lithium insertion sites and not interparticle electron transfer. In conclusion, the increased resistance that results from increased interparticle contacts at low temperature seems to be the most reasonable explanation for the transition.

Thus we propose that, whereas, we can obtain improved performance under most circumstances with smaller particle size, one must be concerned with the number and nature of interfaces that are created by use of nanoparticle electrodes. We will view this as an opportunity to further improve the electrode properties of nanophase $Li_4Ti_5O_{12}$ by creating a nanostructured material with short diffusion lengths and a limited number of interfaces. An example of an electrode material (V_2O_5) with nanometer dimensions and limited number of interfaces has been reported by Sides and Martin [9]. Sides and Martin prepared V_2O_5 "nanorod" electrodes, which demonstrated extremely good low temperature performance. The nanorod architecture (nanometer diameter, micrometer length rods) may be preferable to nanoparticle because the advantages of high surface area and short diffusion lengths are present, however, there are many fewer interparticle contacts in a nanorod than in a nanoparticle and so one does not introduce increased interparticle contacts when scaling down to the nanoscale. Similarly, a porous material may have similar advantages for charge transport applications [21]. Further, it points to the need to evaluate the electrode manufacturing process in order to gain the most benefit from the use of nanoparticle sized electrode materials, that is, one can not simply view this as a drop-in technology.

4. Conclusions

The properties of 350 and 700 nm $Li_4Ti_5O_{12}$ anodes were investigated with an emphasis on low temperature performance. The 350 nm $Li_4Ti_5O_{12}$ material exhibited higher capacity as a result of its shorter diffusion lengths and higher number of lithium insertion sites compared to the 700 nm $Li_4Ti_5O_{12}$ at all rates tested at room temperature or at low rate and low temperature. There is, however, a cross-over in performance occurring at high rate and low temperature. It is suggested that the origin of the transition is related to the higher number of interparticle contacts in the 350 nm material versus the 700 nm material. It is believed that as temperature is lowered the resistance of the interparticle contacts increases and controls the discharge rate. This suggests the possibility to further optimize the nanophase $Li_4Ti_5O_{12}$ anode material through preparation of $Li_4Ti_5O_{12}$ materials in which the short, nanometer scale diffusion lengths are preserved while minimizing the number of interparticle interfaces. A clear advantage may be envisioned for such a nanostructured material.

Acknowledgments

The authors kindly thank ARL colleagues, J. Molstad (SEM), W. Sarney (TEM) and I. Lee (BET), for assistance with obtaining particle size information and A. Singhal of NEI for providing the NEI-$Li_4Ti_5O_{12}$ sample. The Army Research Laboratory is acknowledged for financial support of this research.

References

[1] K.M. Colbow, J.R. Dahn, R.R. Haering, J. Power Sources 26 (1989) 397.
[2] E. Ferg, R.J. Gummov, A. de Kock, M.M. Thackeray, J. Electrochem. Soc. 141 (1994) L147.
[3] T. Ohzuku, A. Ueda, N. Yamamoto, J. Electrochem. Soc. 142 (1995) 1431.
[4] G.G. Amatucci, F. Badway, A. Du Pasquier, T. Zheng, J. Electrochem. Soc. 148 (2001) A930.
[5] A. Du Pasquier, A. Laforgue, P. Simon, G.G. Amatucci, J.F. Fauvarque, J. Electrochem. Soc. 143 (2002) 394.
[6] L. Kavan, J. Procházka, T.M. Spitler, M. Kalbáč, M. Zukalová, T. Drezen, M. Grätzel, J. Electrochem. Soc. 150 (2003) A1000.
[7] C.-K. Huang, J.S. Sakamoto, S. Surampudi, J. Wolfenstine, Abstract 369, The Electrochemical Society and International Society of Electrochemistry Meeting Abstracts, vol. 99–102, Honolulu, HI, October 17–22, 1999.
[8] C.-K. Huang, J.S. Sakamoto, J. Wolfenstine, S. Surampudi, J. Electrochem. Soc. 147 (2000) 2893.
[9] C.R. Sides, C.R. Martin, Adv. Mater. 17 (2005) 125.
[10] A. Singhal, G. Skandan, U.S. Patent 6,827,921, 2004.
[11] A. Deschanvers, B. Raveau, Z. Sekkal, Mater. Res. Bull. 6 (1971) 699.
[12] H.M. Rietveld, J. Appl. Crystallogr. 2 (1969) 65–71.
[13] S. Brunauer, P.H. Emmett, E. Teller, J. Am. Chem. Soc. 60 (1938) 309.
[14] L. Kavan, M. Grätzel, Electrochem. Solid-State Lett. 5 (2002) A39.
[15] M. Kalbáč, M. Zukalová, L. Kavan, J. Solid State Electrochem. 8 (2003) 2.

[16] M.R. Harrison, P.P. Edwards, J.B. Goodenough, Philos. Magn. B 52 (1985) 679.
[17] A.R. West, Solid State Chemistry and its Applications, John Wiley and Sons, New York, 1984, pp. 173–175.
[18] J.D. Corbett, in: A.K. Cheetham, P. Day (Eds.), Solid State Chemistry: Techniques, Clarendon Press, Oxford, 1987, pp. 21–22.
[19] K. Xu, Chem. Rev. 104 (2004) 4303.
[20] A.R. West, Solid State Chemistry and its Applications, John Wiley and Sons, New York, 1984, pp. 497–498.
[21] J.W. Long, B. Dunn, D.R. Rolison, H.S. White, Chem. Rev. 104 (2004) 4463.